ACS APPLIED MATERIALS & INTERFACES

Research Article

www.acsami.org

Selective Capture of Iodide from Solutions by Microrosette-like δ-Bi_2O_3

Long Liu,[†] Wei Liu,[‡] Xiaoliang Zhao,[†] Daimei Chen,[§] Rongsheng Cai,[†] Weiyou Yang,*[,⊥] Sridhar Komarneni,[#] and Dongjiang Yang*[,†,∥]

[†]Collaborative Innovation Center for Marine Biomass Fibers, Materials and Textiles of Shandong Province, College of Chemistry, Chemical and Environmental Engineering, and [‡]Library of Qingdao University, Qingdao University, Qingdao 266071, China

[§]National Laboratory of Mineral Materials, School of Materials Sciences and Technology, China University of Geosciences, Beijing 100083, China

[⊥]Institute of Materials, Ningbo University of Technology, Ningbo City 315016, P.R. China

[#]Materials Research Institute and Department of Ecosystem Science and Management, The Pennsylvania State University, University Park, Pennsylvania 16802, United States

[∥]Queensland Micro- and Nanotechnology Centre (QMNC), Griffith University, Nathan, Brisbane, QLD 4111, Australia

Supporting Information

ABSTRACT: Radioactive iodine isotopes that are produced in nuclear power plants and used in medical research institutes could be a serious threat to the health of many people if accidentally released to the environment because the thyroid gland can absorb and concentrate them from a liquid. For this reason, uptake of iodide anions was investigated on microrosette-like δ-Bi_2O_3 (MR-δ-Bi_2O_3). The MR-δ-Bi_2O_3 adsorbent showed a very high uptake capacity of 1.44 mmol g^{-1} by forming insoluble $Bi_4I_2O_5$ phase. The MR-δ-Bi_2O_3 also displayed fast uptake kinetics and could be easily separated from a liquid after use because of its novel morphology. In addition, the adsorbent showed excellent selectivity for I^- anions in the presence of large concentrations of competitive anions such as Cl^- and CO_3^{2-}, and could work in a wide pH range of 4−11. This study led to a new and highly efficient Bi-based adsorbent for iodide capture from solutions.

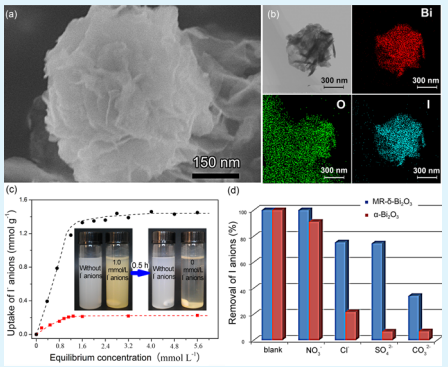

KEYWORDS: *δ-Bi_2O_3, adsorbent, iodide uptake, $Bi_4I_2O_5$, radioactive waste, selectivity*

1. INTRODUCTION

Radioiodine is an inevitable product of nuclear fission, which is highly radioactive and acutely toxic, and could present a health risk upon people once it is released to the environment. The half-life of radioiodine differs from about 8 days (^{131}I) to 1.6 × 10^7 years (^{129}I), and its potential toxicity is due to bioaccumulation through the food chain and subsequent dysfunction of the thyroid gland.[1,2] In the 1950s, open-air atomic bomb testing released a large amount of radioisotope of iodides such as ^{131}I. Furthermore, the nuclear power plant accidents such as Chernobyl and Fukushima disasters resulted in the leakage of radioactive iodides.[3−6] In addition to the release from nuclear power plants, radioactive iodine has also been used in the treatment of thyroid cancer and as a result, radioactive wastewater is discharged by numerous medical research institutes.[7−9] For instance, ^{131}I, a radionuclide widely used in hyperthyroidism, thyroid cancer diagnosis and metabolic therapies,[10] is habitually dumped into domestic sewer systems and it is one of the radioactive species most often detected in the drain outlet.[11−14] In addition to a tiny amount of iodate ions in highly oxidizing aqueous environment, iodine is present in the −1 valence state as the iodide anion (I^-) and is stable almost over the entire pH range.

Various methods have recently been proposed to immobilize these carcinogenic substances onto organic[15,16] or inorganic compounds.[17−19] For instance, anion exchange resin[20] and compounds containing Bi(III),[21] Pb(II),[22] Hg(II),[23] Ag(I),[24] and Cu(I)[23,25,26] have been reported as adsorbents to remove the radioactive ^{131}I ions from waste streams at nuclear power plants. However, organic materials like resin are unstable under high dose of radiation and elevated temperatures, whereas the inorganic materials are of relatively low adsorption capacities with extremely slow uptake kinetics because of small specific surface area. More recently, we reported a novel adsorbent structure for the highly efficient and selective capture of radioactive iodine from water, where silver oxides (Ag_2O) nanocrystals which play a role as immobilization center for I^- were anchored onto the surface of titanate nanostructures (i.e., nanofibers, nanotubes, and nanosheets).[27−30] The I^- anions in

Received: June 23, 2014
Accepted: August 29, 2014
Published: August 29, 2014

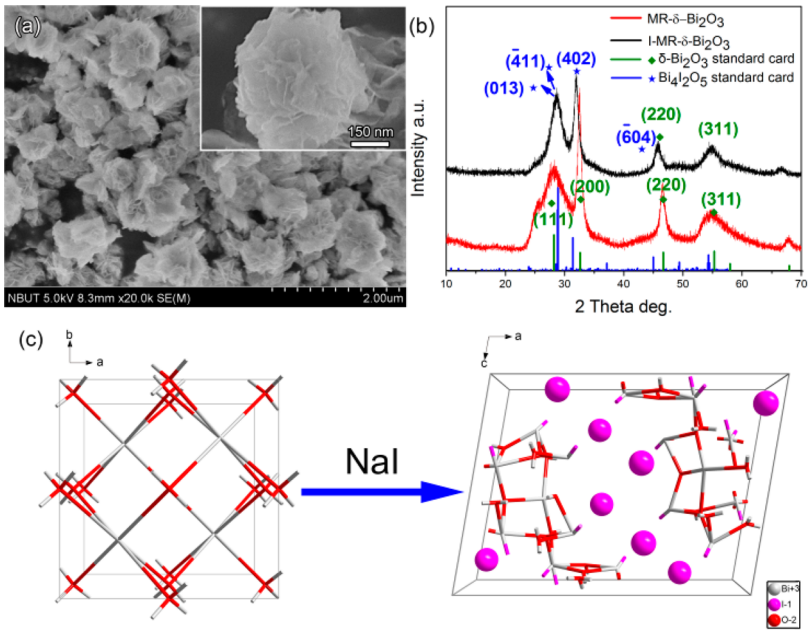

Figure 1. (a) SEM images of the as-obtained MR-δ-Bi_2O_3 adsorbent at low magnification, inset: a feature of individual flowerlike structure at high magnification; (b) XRD patterns of the adsorbent before and after iodide anion adsorption; (c) schematic illustration of the conversion of δ-Bi_2O_3 to the $Bi_4I_2O_5$ structure.

fluids can easily access the Ag_2O nanocrystals and be efficiently trapped by forming AgI precipitate that tightly attaches to the adsorbent. The adsorption capacities of $^{125}I^-$ anions by the Ag_2O-based adsorbents are as high as 4.5 mmol per gram.[27−30] Furthermore, Nenoff and co-workers have developed layered hydrotalcite-like Bi-I-oxides as waste forms for I^- anions precipitation.[31,32] It was found that the phase composition and I weight loading of the Bi−I−O are determined by the Bi:I ratio in an acidified Bi nitrate solution. This finding highlighted new direction for in situ precipitation synthesis of Bi-based radioactive iodine waste forms.

Although Ag_2O-based adsorbents displayed high adsorption capacity and selectivity for radioactive I^- anions, the high costs of silver limits its practical application.[33] Herein, microrosette-like δ-Bi_2O_3 (hereafter, microrosette-like δ-Bi_2O_3 is referred to as MR-δ-Bi_2O_3) was fabricated via a simple hydrothermal process in the presence of glycine and bismuth nitrate pentahydrate as the raw materials.[34] It was found that the MR-δ-Bi_2O_3 could quickly react with I^- anions by forming $Bi_4I_2O_5$ microcrystals and its sorption capacity is as high as ~1.44 mmol g^{-1}. Compared with other iodide sorption materials, the MR-δ-Bi_2O_3 adsorbent shows good performance in high uptake capacity with fast kinetic and high selectivity (see Table S1 in the Supporting Information). In addition, the large microsized δ-Bi_2O_3 substrate could be easily separated from water by facile sedimentation process. Compared with the expensive Ag_2O nanocrystal-based adsorbents, the δ-Bi_2O_3 adsorbent could be more economical and promising for practical application.

2. EXPERIMENTAL SECTION

2.1. Preparation of MR-δ-Bi_2O_3. The MR-δ-Bi_2O_3 material was fabricated via a facile hydrothermal method.[32,35] A typical synthesis procedure is as follows. First, 4 mmol $Bi(NO_3)_3{\cdot}5H_2O$ (Sinopharm Chemical Reagent Co., Ltd. ≥99.0%) and 20 mmol NH_2CH_2COOH (Aladdin Chemistry Co. Ltd. ≥99.0%) were dissolved in 60 mL deionized water, followed by vigorous stirring for 5 min at room temperature. Subsequently, the mixture was sonicated for 30 min by an ultrasonic generator. The mixture was put into a Teflon-lined stainless steel autoclave with a capacity of 100 mL. The autoclave was sealed and heated at 140 °C for 24 h. Then, the autoclave was cooled to room temperature naturally. Finally, the products were washed with absolute ethanol and deionized water several times followed by drying under vacuum at 60 °C for 24 h.

2.2. Equilibrium Adsorption Test. In the present study, the anion adsorption experiments were carried out with nonradioactive $^{127}I^-$ (NaI) in aqueous solution because of the high radiation dose and toxicity of ^{131}I & ^{129}I. The equilibrium uptake capacities of the MR-δ-Bi_2O_3 sorbents for I^- anions were conducted through batch experiments which were implemented using a series of concentrations of I^- anion solutions ranging from 1 μmol L^{-1} to 10 mmol L^{-1} (the amount of adsorbent = 1 g L^{-1}, 25 °C, pH = 6.5). For comparison, the same amount of α-Bi_2O_3 (purchased from Aladdin Chemistry Co. Ltd. ≥99.0%, the mean grain size is below 1 μm) was used as a control. All the samples with iodide solutions were equilibrated for over 48 h at room temperature with magnetic stirring. Afterward the solids and solutions were separated by centrifugation and the supernatants were analyzed by ultraviolet spectrophotometer (UV−vis) to determine the remaining iodide anions in the solutions.[30]

2.3. Kinetics of Adsorption. The kinetics of I^- adsorption by MR-δ-Bi_2O_3 were determined using iodide concentrations of 0.4, 0.8, and 1.2 mmol L^{-1} (the amount of adsorbent = 1 g L^{-1}, 25 °C, pH = 6.5). The suspensions were equilibrated for different periods while stirring at room temperature. After appropriate time interval, the supernatants were separated from solids and analyzed as described above.

2.4. Selective Adsorption and the Influence of pH on I^- Immobilization. The selective uptake of I^- anions by MR-δ-Bi_2O_3 adsorbent in the presence of high concentrations of Cl^-, NO_3^-, SO_4^{2-}, and CO_3^{2-} anions was investigated. Briefly, 50 mg of adsorbent was dispersed into 50 mL aqueous mixture solution containing 80 μmol L^{-1} NaI and 80 mmol L^{-1} of Cl^-, NO_3^-, SO_4^{2-}, or CO_3^{2-} anions. Uptake of I^- anions as a function of solution pH ranging from 4 to 11 was also done by adjusting the pH with dilute HNO_3 and $NH_3{\cdot}H_2O$ solutions with the initial concentration of I^- set at 0.4 mmol L^{-1}.

2.5. Desorption Test of the Precipitated I^- anions. Leaching or desorption was examined in various aqueous solutions. The 20 mg of adsorbents saturated with I^- anions were collected via the

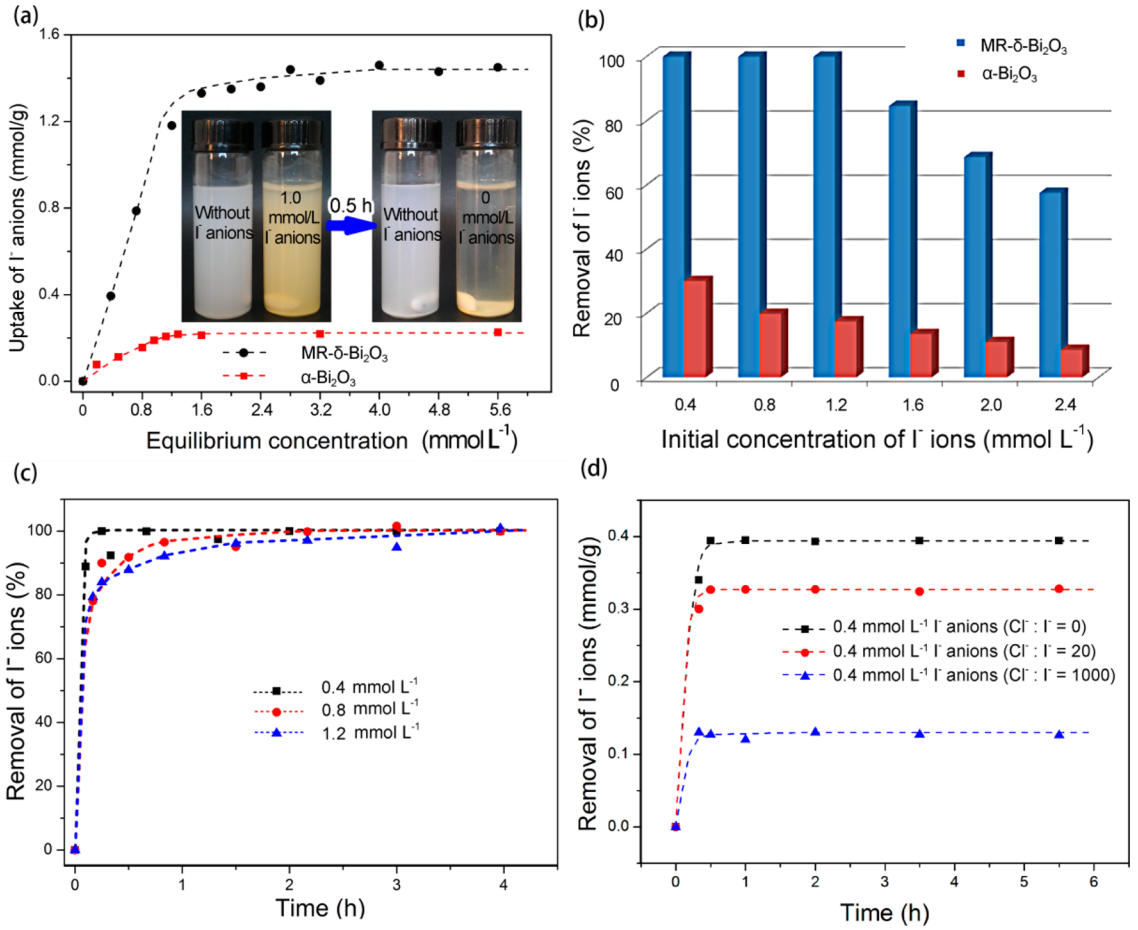

Figure 2. Removal of iodide anions from solutions by MR-δ-Bi_2O_3. (a) The isotherms of I^- uptake by MR-δ-Bi_2O_3 and α-Bi_2O_3 over 48 h (25 °C, pH = 6.5). The photo in the inset depicts the adsorbent in I^- aqueous solution (left) and sedimentation changes after 30 min (right) and the deionized water was set as a control. (b) Removal of I^- anions as a function of the anion concentration in water. (c) I^- adsorption kinetics of MR-δ-Bi_2O_3. (d) I^- adsorption kinetics in 0.4 mmol L^{-1} I^- anions with different concentrations of Cl^- as a competitive anion.

centrifugation and rinsed with deionized water three times to remove the remaining I^- in the solution and the adsorbents were redispersed into 20 mL of different concentration NaCl and Na_2CO_3 solutions. The suspension was stirred for more than 48 h at room temperature and the I^- anion concentrations of the solutions were determined by UV−vis spectroscopy as described above.

2.6. Characterization. The micromorphologies of the samples before and after sorption of I^- anions were obtained on a scanning electron microscope (SEM; Hitachi, S-4800 with an accelerating voltage of 5 kV). The composition of the sample after adsorption of iodide anions was determined by energy-dispersive X-ray (EDX) spectroscopy attached on the same microscope. High-resolution transmission electron microscopy (HRTEM) images were taken on a JEOL JEM-2100F field emission electron microscope under an accelerating voltage of 200 kV. The crystallized phases were identified by powder X-ray diffraction (XRD) analysis using an X-ray diffractometer (DX-2700, China) with Ni-filtered Cu Kα radiation (λ = 1.5406 Å) at 40 kV and 30 mA with a fixed slit. The Brunauer−Emmett−Teller (BET) specific surface area was measured by using nitrogen adsorption on a Micromeritics TriStar surface area and porosity analyzer. The X-ray photoelectron spectroscopy (XPS) data were obtained on a Kratos Axis Ultra DLD electron spectrometer using 150 W Al Kα radiation. Raman spectra were recorded on a microscopic confocal Raman spectrometer (Renishaw 1000 NR) with an excitation of 514.5 nm laser light. Besides, the iodide anion adsorption value was obtained via UV−vis. The filtrate was analyzed by UV−vis spectroscopy (MAPADA 3200PC Spectrometer) for the absorbance intensity using a reading at 227 nm.

3. RESULTS AND DISCUSSION

3.1. Structure and Morphology of Phases. The morphologies of the hydrothermally synthesized hierarchical δ-Bi_2O_3 rosette structures were examined by SEM (Figure 1). A typical low-magnification SEM image of the as-synthesized MR-δ-Bi_2O_3 (Figure 1a) clearly reveals that the sample consists of fluffy flower-like microspheres with an average diameter of 0.4−0.6 μm with a specific surface area of 24.4 m^2 g^{-1} by the Brunauer−Emmett−Teller (BET) method (see Figure S2 in the Supporting Information). Furthermore, the enlarged SEM image (inset in Figure 1a) demonstrates that the fluffy flowerlike microspheres were assembled by large number of nanosheets. Powder XRD pattern (Figure 1b) shows many characteristic peaks, which can be indexed as δ-Bi_2O_3 crystalline phase (JCPDS, Card No. 27−0052). Additionally, the HRTEM investigation demonstrates that the nanosheets were assembled from numerous nanoparticles (see Figure S1a in the Supporting Information), i.e., the substructure of the nanosheets is sphere architecture and the exposed plane of these nanoparticles is (111) plane (see Figure S1b−d in the Supporting Information).

3.2. Adsorption Isotherm. The I^- anion equilibrium uptake isotherm of MR-δ-Bi_2O_3 is shown in Figure 2a. This isotherm suggests that the maximum uptake capacity of MR-δ-Bi_2O_3 can reach up to 1.44 mmol g^{-1}. However, the uptake capacity of commercial α-Bi_2O_3 is only 0.22 mmol g^{-1}. The uptake capacity of the MR-δ-Bi_2O_3 compound is much higher

than that of the Cu(I) based adsorbents. For instance, the maximum capacity of copper(I) sulfide minerals is ~48 μmol g^{-1} and that of the Cu_2O mineral is as low as 2 μmol g^{-1} (see Table S1 in the Supporting Information).[25,26] As shown in Figure 2b, the iodide anions with a concentration of ≤1.2 mmol L^{-1} can be completely removed by the MR-δ-Bi_2O_3 adsorbent, and about 84.6% of iodide anions were taken up when the concentration of iodide anions was at 1.6 mmol L^{-1}. Besides, its capacity of adsorption increases with temperature rising (see Figure S4 in the Supporting Information). As shown in the inset photo of Figure 2a, the white MR-δ-Bi_2O_3 adsorbent turned to bright yellow color after the sorption of I^- anions. According to the XRD pattern in Figure 1b, a new phase indexed as $Bi_4I_2O_5$ formed during the uptake process,[36] which can be explained by eq 1[37]

$$Bi_2O_3(s) + I^-(aq) + (1/2)H_2O(I) \rightarrow (1/2)Bi_4I_2O_5(s) + OH^-(aq) \quad (1)$$

This result is different from that previously reported by Tayler et al.,[21] where insoluble Bi_5O_7I was formed after the capture of I^- anions. Furthermore, the $Bi_4I_2O_5$/MR-δ-Bi_2O_3 composite exhibits high stability to thermal treatment. For instance, the composite will convert to Bi_5O_7I when it is heated higher than 300 °C (see Figure S5 and eq S1 in the Supporting Information). This property avoids the release of the adsorbed iodine during the radioactive waste disposal process (see eq S1 in the Supporting Information).

The interaction between adsorbent and iodate ions (IO_3^-) in solution was also explored. Unfortunately, there is no change observed from the XRD pattern of the adsorbent collected from the KIO_3 solution compared with the pristine MR-δ-Bi_2O_3 adsorbent (see Figure S6 in the Supporting Information). This result is in sharp contrast to the situation in NaI solution. In addition, compared to the sharp color contrast after interaction with NaI solution (see Figure S7a in the Supporting Information), the color of the adsorbent remained constant in the KIO_3 solution (see Figure S7b in the Supporting Information). So on the basis of this study, it can be concluded that the MR-δ-Bi_2O_3 adsorbent is not able to capture IO_3^- ions from an aqueous solution.

3.3. Structural Evolution of Used Adsorbent. The adsorbent after uptake of I^- anions was washed and characterized by TEM. As shown in Figure 3a, the adsorbent appears to maintain the flower-like morphology after the uptake of iodide. The EDP in Figure 3b demonstrates the existence of both cubic δ-Bi_2O_3 phase and monoclinic $Bi_4I_2O_5$ phase, which is in good agreement with the XRD data. As can be seen from Figure 3c, one set of the fringe spacing of 0.291 nm is corresponding to the (312) plane of the monoclinic $Bi_4I_2O_5$. The other fringe spacing of 0.319 nm in Figure 3d belongs to the (111) plane of cubic δ-Bi_2O_3 phase. Moreover, some stacking faults (SFs) were observed after reaction of I^- anions from the HRTEM image of the lattice of the MR-δ-Bi_2O_3 adsorbent (Figure 3d). However, these stacking faults could hardly be detected from the lattice of the MR-δ-Bi_2O_3 adsorbent before adsorption (see Figure S1c, d in the Supporting Information). This could be ascribed to the huge difference in structure between cubic δ-Bi_2O_3 and monoclinic $Bi_4I_2O_5$. As shown in Figure 1b, the numerous SFs result in the disappearance of diffraction peaks at 27.9 and 32.3°, which are assigned to (111) and (200) planes of δ-Bi_2O_3.

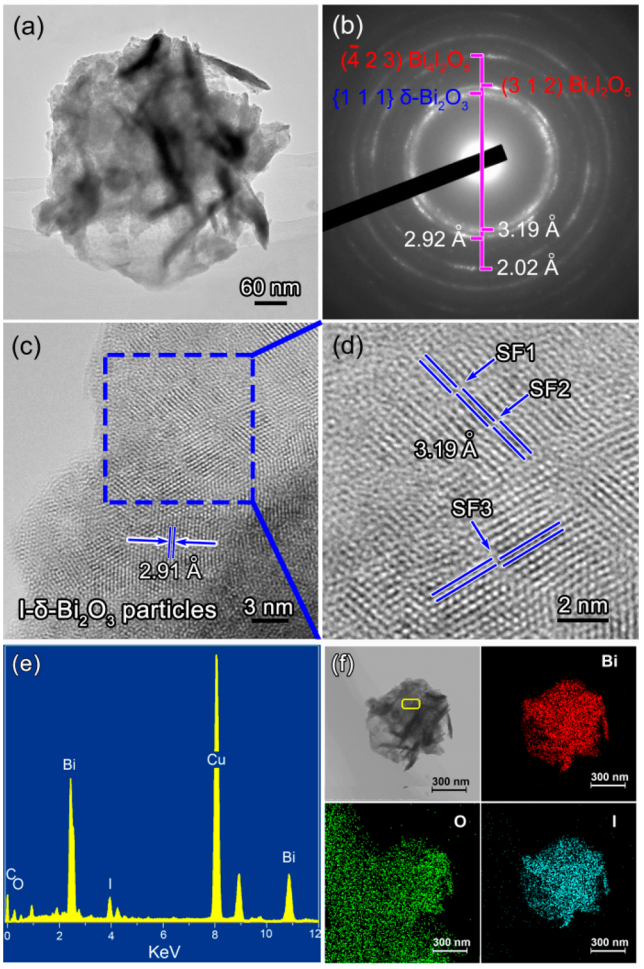

Figure 3. TEM images of I-MR-δ-Bi_2O_3. (a) TEM image at low magnification shows that the used adsorbent retained the same morphology after uptake of iodide. (b) Electron diffraction rings of the I-δ-Bi_2O_3. (c) HRTEM image of the mixed-phase of nanoparticles. (d) The enlarged image with three obvious stacking faults. (e) EDX patterns of the selected area in TEM image of the used sorbent particles showing iodine. (f) Elemental mapping of the particles in the TEM image.

The XPS analysis of adsorbent before and after use was performed for the composition analysis of the samples. Figure 4 is a typical XPS survey spectrum and high-resolution XPS spectra of different atoms. Before adsorption of I^- anions, the two strong peaks at Bi region of 158.8 and 164.1 eV are assigned to Bi $4f_{7/2}$ and Bi $4f_{5/2}$ (Figure 4b), respectively, which are characteristics of Bi^{3+}.[38] The O 1s core level spectrum (Figure 4c) can be fitted well with two peaks. The peak at 529.5 eV is characteristic of a bismuth−oxygen bond in Bi_2O_3,[39] and the other peak at 531.8 eV is attributed to the chemisorbed H_2O or OH^- on the surface, respectively. After adsorption of I^- anions by forming $Bi_4I_2O_5$ on the surface, the I 3d core level appears at the binding energies of around 630.2 eV (I $3d_{3/2}$) and 618.7 eV (I $3d_{5/2}$), respectively (Figure 4f), which is in good agreement with those reported in other bismuth oxideiodides.[40,41] At the meantime, the O 1s spectrum of the adsorbent after I^- anions adsorption is quite different. As shown in Figure 4e, the main peak at 529.5 eV (Bi−O) remains after uptake of I^- anions, and the peak at 531.4 eV (OH) becomes weak substantially. Additionally, the newly formed

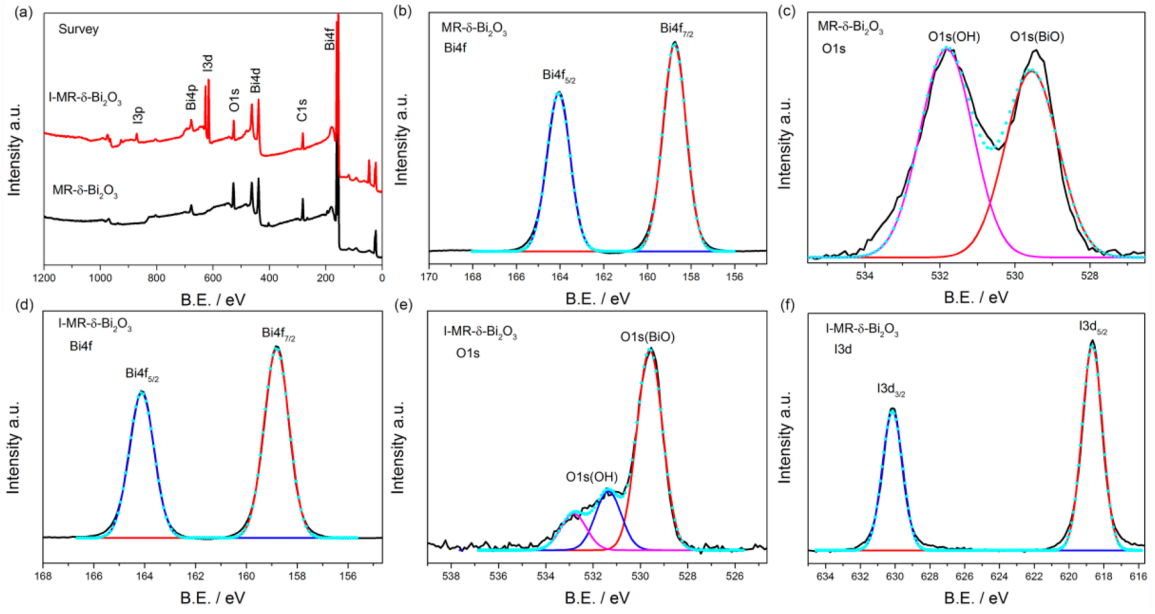

Figure 4. XPS spectra of MR-δ-Bi_2O_3 adsorbent before and after uptake of I^- anions: (a) survey scan; (b) Bi_{4f} and (c) O_{1s} of MR-δ-Bi_2O_3; (d) Bi_{4f}, (e) O_{1s}, and (f) I_{3d} of I-MR-δ-Bi_2O_3.

weakest peak at 532.8 eV should be ascribed to the CO_2 molecules adsorbed on the surface of adsorbent.[42,43]

The Raman spectra of MR-δ-Bi_2O_3 and I-MR-δ-Bi_2O_3 are displayed in Figure 5. Apparently, a well-defined peak below

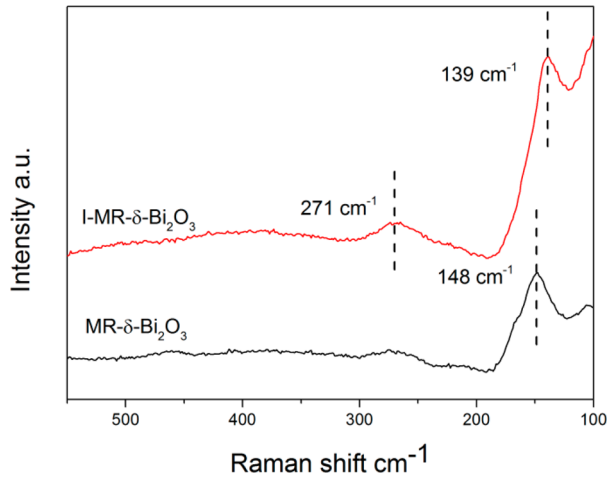

Figure 5. Raman spectra of MR-δ-Bi_2O_3 adsorbent before and after uptake of I^- anions.

200 cm^{-1} has been detected from the hydrothermally synthesized MR-δ-Bi_2O_3, which is assigned to lattice vibrations (external modes are characteristically sharper than internal modes).[44] This result is similar to that of the niobium or tantalum-doped δ-Bi_2O_3 system,[44] and is quite different from that δ-Bi_2O_3 films whose characteristic peak is at 618 cm^{-1}.[45,46] After uptake of I^- anions, the main peak of the MR-δ-Bi_2O_3 adsorbent shifts from 148 to 139 cm^{-1}, caused by the Bi–I external symmetric stretching vibration.[47,48] Meanwhile, a weak broad band appears at 271 cm^{-1}, which is assigned to modes involving motion of the adsorbed iodine atoms.[48]

3.4. Uptake Kinetics. The kinetics of the I^- uptake by the MR-δ-Bi_2O_3 adsorbent are plotted for different I^- anion concentrations of 0.4, 0.80, and 1.2 mmol L^{-1} as shown in Figure 2c. The removal percentage for I^- anions reached 100, 90, and 84% on MR-δ-Bi_2O_3 in the first 15 min at the initial concentration of 0.4, 0.8, 1.2 mmol L^{-1}, respectively, and the I^- anions could be captured completely in 90 min (Figure 2c). Compared with the kinetics of traditional Cu and Pb-based adsorbents,[22,26] the MR-δ-Bi_2O_3 adsorbent is faster and thus more efficient in terms of sorption kinetics for the removal of I^- anions. The high adsorption kinetics could be ascribed to the nanosheet assembled fluffy structure of the MR-δ-Bi_2O_3. First, the I^- anions were easily accessed by the δ-Bi_2O_3 nanosheets through the fluffy structure. As shown in the inset of Figure 2a, the rosette-like adsorbents can readily disperse in the solution of I^- anions. Second, the δ-Bi_2O_3 nanosheets composed of nanoparticles were more reactive with the I^- anions compared with the conventional microsized adsorbents. In addition, the adsorbent maintained rosette morphology after the sorption of I^- anions (see Figure S3b in the Supporting Information), which assures that the adsorbents can settle down in 30 min for facile separation of the adsorbents from solutions for ultimate safe disposal (inset of Figure 2a). This property could significantly reduce the cost of the separation and make it feasible for practical application.

Furthermore, the adsorption kinetics was explained by the pseudo-second order model[49] given as follows

$$\frac{dq}{dt} = k_2(q_e - q)^2 \tag{2}$$

Where k_2 (g $mmol^{-1}$ h^{-1}) is the second-order rate constant. Integrating for the boundary conditions $q = 0$ to $q = q_t$ at $t = 0$ to $t = t$ is simplified as

$$\frac{t}{q_t} = \frac{1}{k_2 q_e^2} + \frac{1}{q_e}t \tag{3}$$

$$h = k_2 q_e^2 \tag{4}$$

where q_t (mmol/g) represents the adsorption capacity at t (h), h is the initial sorption rate (mmol g^{-1} h^{-1}); k_2 and q_e can be obtained from the intercept and slope of plotting t/q_t versus t.

dx.doi.org/10.1021/am504000n | ACS Appl. Mater. Interfaces 2014, 6, 16082–16090

The initial adsorption rate (h), the equilibrium adsorption capacity (q_e) and the pseudo-order rate constants k_2 are obtained from the slope and intercept of the plots of t/q_t against t.

The plot t/q_t versus t for various I^- concentrations is shown in Figure 6 and the pseudo-second-order adsorption rate

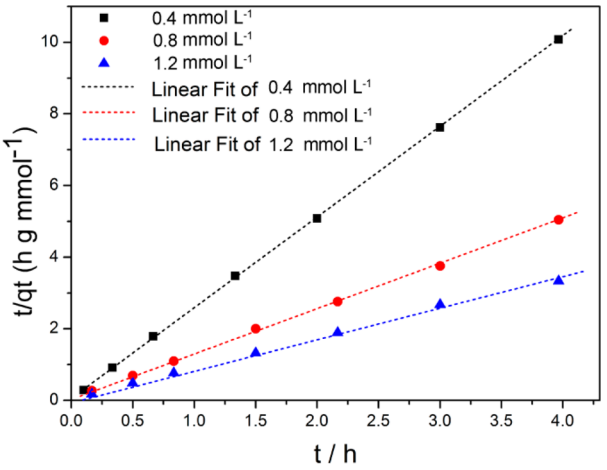

Figure 6. Pseudo-second-order kinetics model for iodide anion adsorption on the MR-δ-Bi_2O_3 adsorbent.

constants for different initial concentrations were summarized in Table 1. It was observed that the pseudo-second-order rate

Table 1. Pseudo-second-order Adsorption Rate Constants at Different Initial Concentrations

	pseudo-second-order			
C_0 (mmol L^{-1})	K_2 (g $mmol^{-1}$ h^{-1})	h (mmol g^{-1} h^{-1})	R^2	q_e (cal) (mmol g^{-1})
0.4	86	13.7	1	0.40
0.8	22	14.01	0.999	0.80
1.2	11	16.04	0.998	1.19

constant (k_2) decreased, whereas the initial adsorption rate (h) increased with increased initial I^- concentration. The adsorption was analyzed by using pseudo-second-order kinetic model which is used to predict the kinetic behavior of adsorption with chemical adsorption being the rate controlling step.[50] As displayed in Figure 6 and Table 1, the estimated equilibrium adsorption capacities at 0.4, 0.8, and 1.2 mmol L^{-1} were 0.40, 0.8, and 1.19 mmol g^{-1}, respectively, which are in good agreement with the experimental results.

3.5. Selective Uptake and Leaching Test. To investigate the selective uptake of I^- anions by the MR-δ-Bi_2O_3 adsorbent, we conducted the uptake test in the presence of high concentrations of Cl^-, SO_4^{2-}, CO_3^{2-}, and NO_3^- anions. As shown in Figure 2d, the uptake of I^- anions was lower as the concentration of Cl^- anions increased. For instance, 83.3% and 32.6% of the I^- anions could be collected by the MR-δ-Bi_2O_3 adsorbent, when the concentration of Cl^- anions were 20 and 1000 times of the I^- anions (0.4 mmol L^{-1}), respectively. The influence of a large excess of Cl^-, SO_4^{2-}, CO_3^{2-}, and NO_3^- (80 mmol L^{-1}) on the uptake of I^- anions (80 μmol L^{-1}) is illustrated in Figure 7a. Apparently, more than 99% of the I^- anions were removed from the NO_3^- solutions, whereas the I^- uptake values were 75.2, 74.4, and 34% for the Cl^-, SO_4^{2-}, and CO_3^{2-} competitive anions, respectively. In comparison with that of the commercial α-Bi_2O_3 (Figure 7a), the uptake selectivity of MR-δ-Bi_2O_3 is excellent. To elucidate the adsorption selectivity of MR-δ-Bi_2O_3, the hydrolysis process of $Bi_4I_2O_5$ in the presence of Cl^- or CO_3^{2-} anions was analyzed (see the effect of competitive anions on $Bi_4I_2O_5$ waste form in the Supporting Information). The thermodynamic calculation exhibited that the Gibbs energy for the reaction between MR-δ-Bi_2O_3 and I^- anions is lower than that for the reaction between MR-δ-Bi_2O_3 and Cl^-, but it is higher than that for the reaction between MR-δ-Bi_2O_3 and CO_3^{2-} (see the reaction energy calculation of MR-δ-Bi_2O_3 and NaI (or NaCl/$NaCO_3$) in the Supporting Information). Thus, the MR-δ-Bi_2O_3 adsorbent displayed higher selectivity for Cl^- than CO_3^{2-}. For instance, the selective sorption percentage of MR-δ-Bi_2O_3 can reach 96% at pH = 6.5 (C_{Cl}:C_I = 1000), higher than that of previously reported Bi_5O_7I (93%) or BiOI (<10%) (see Table S1 in the Supporting Information).[31] For these sorption materials, the equilibrium concentrations of I^- anions as a function of pH and competitive anions were summarized in equations S28−35 in the Supporting Information. It was found that $Bi_4I_2O_5$ (MR-δ-Bi_2O_3) shows more advantageous toward I^- selective capture than that of Bi_5O_7I or BiOI. In addition, the I^- anion leaching

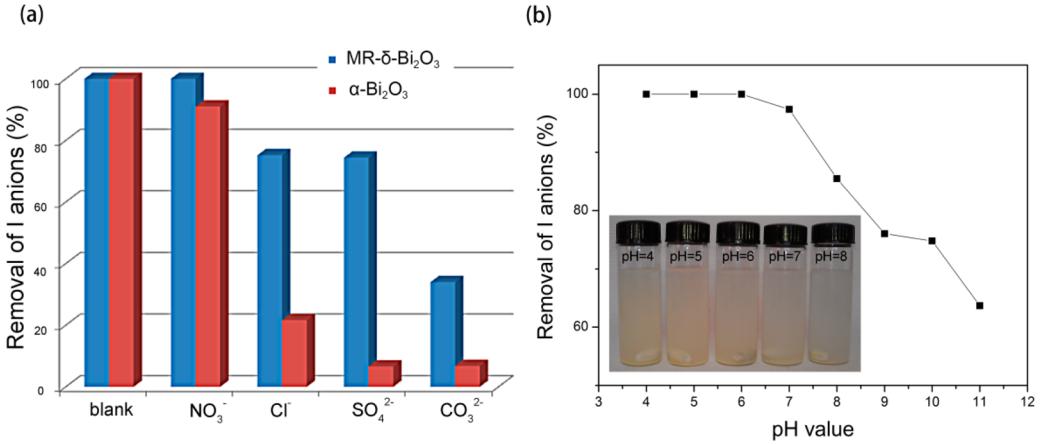

Figure 7. Influence of competitive anions and pH on uptake. (a) Effect of high concentration of NO_3^-, Cl^-, SO_4^{2-}, and CO_3^{2-} on the removal of I^- anions by MR-δ-Bi_2O_3 and α-Bi_2O_3 (competitive anions is 1000 times higher than that of I^- in molar ratio). (b) Immobilization percentage of I^- anions in the pH range of 4 to 11. Inset: color change of suspension in different pH environments.

amount from Bi_5O_7I that is formed on the surface of the α-Bi_2O_3 adsorbent[31,51] is larger than that of $Bi_4I_2O_5$ under the condition of competitive anions. So compared with commercial α-Bi_2O_3, the MR-δ-Bi_2O_3 has a superior ability of antisolubility in high concentration of competitive anions.

Furthermore, leaching or desorption tests of the used adsorbent were conducted to evaluate the sorption reversibility of the MR-δ-Bi_2O_3 adsorbent. Sorption irreversibility is desirable for radioactive waste treatment since it can ensure the release of the adsorbed radioactive species and thus avoid the resultant secondary pollution. The iodide ions are irreversibly adsorbed, and hence they need not be made into a ceramic or glass waste form but can be disposed of separately if it cannot be incorporated in ceramic or glass waste form. Similar to the adsorption selectivity, the leaching behavior is important when the leaching is solubility controlled. We found that the quantity of the I^- anions released into pure water from a used sample is very low or below the detection limits, and the I^- anion release was almost not affected with the temperature rising (see Figure S4 in the Supporting Information). However, as shown in Table 2, the presence of small amounts of Cl^- or

Table 2. Desorption Percentage of I^- Anions in the Presence of Cl^- and CO_3^{2-} Anions (pH = 6, 298 K), respectively

C_{NaCl} (mol L^{-1})	equilibrium I^- (mol L^{-1})	C_{NaCO3} (mol L^{-1})	equilibrium I^- (mol L^{-1})
1×10^{-5}	$<1 \times 10^{-6}$	1×10^{-7}	1.1×10^{-6}
1×10^{-4}	1.3×10^{-6}	1×10^{-6}	2.2×10^{-5}
5×10^{-4}	5×10^{-6}	5×10^{-6}	5.8×10^{-5}
1×10^{-2}	1.2×10^{-4}	1×10^{-4}	2.6×10^{-4}

CO_3^{2-} anions can cause a slight increase in the amount of leached I^- anions from the MR-δ-Bi_2O_3 adsorbent, and a further increase in Cl^- or CO_3^{2-} anions significantly enhanced the leaching of I^- anions from the used adsorbent.

3.6. Uptake in Weak Acid−Base Medium. To determine the influence of pH on the capture of I^- anions by the adsorbent, we conducted the tests in the pH range of 4−11. As shown in Figure 7b, the uptake efficiencies of MR-δ-Bi_2O_3 decreased with increasing pH, especially in a basic environment. For instance, the I^- anions in 50 mL NaI aqueous solution with concentration of 50 ppm could be completely adsorbed in the pH range of 4−6. However, only 63% of the I^- anions were removed by the MR-δ-Bi_2O_3 adsorbent when the pH value increased to 11. As shown in eq 5, the OH^- ions can participate in the reaction which results in the conversion of newly formed $Bi_4I_2O_5$ to Bi_2O_3. So in weak acid and basic environment, the yellow adsorbent gradually became shallow (inset of Figure 7b). The thermodynamic calculation exhibited that the Gibbs energy for hydrolysis of $Bi_4I_2O_5$ decreases slightly when the pH value increases from 9 to 12 (see the effect of pH values on $Bi_4I_2O_5$ waste form in the Supporting Information). This indicates the amount of the released I^- anions will increase slightly with the pH value increasing, which is in good agreement with the experimental result. Besides, the relationship between equilibrium concentration of the released I^- anions and pH value was calculated to be pI = 15.3 − pH (see eq S10 in the Supporting Information), which means the hydrolysis of $Bi_4I_2O_5$ is extremely sensitive to pH value.

$$Bi_4I_2O_5(s) + 2OH^-(aq) \rightleftharpoons 2Bi_2O_3(s) + 2I^-(aq) + H_2O(l) \quad (5)$$

4. CONCLUSION

In summary, the results presented here confirm that δ-Bi_2O_3 microrosette assembled from nanosheets is an ideal adsorbent for capture of I^- anions from water. For instance, a very high I^- uptake capacity of 1.44 mmol g^{-1} has been achieved. The key to this uptake of I^- anions is to promptly form insoluble $Bi_4I_2O_5$ species on the δ-Bi_2O_3 nanosheet. Additionally, the MR-δ-Bi_2O_3 also displayed fast uptake kinetics and superior selectivity for I^- anions in the presence of large concentrations of competitive anions such as Cl^- and CO_3^{2-}. Given the merits of this adsorbent such as high adsorption capacity, selectivity, and fast kinetics, it may be a cost-effective candidate for the uptake of I^- anions for practical application.

■ ASSOCIATED CONTENT

Supporting Information

Sorption comparative table of the previously published adsorbents (Table S1), equilibrium iodide in solution between $Bi_4I_2O_5$ and Bi_2O_3 at 25 °C (Table S2), TEM images of MR-δ-Bi_2O_3 (Figure S1), SEM images of MR-δ-Bi_2O_3 adsorbent before and after use (Figure S3), BET measurement of adsorbent (Figure S2), effect of temperature on the I^- anions sorption and desorption (Figure S4), phase transition of used sample at high temperature (Figure S5), XRD patterns of the adsorbent before and after interaction with NaI/KIO_3 (Figure S6), color change of the adsorbent before and after interaction with NaI/KIO_3 (Figure S7), reaction energy calculation of MR-δ-Bi_2O_3 and NaI (or NaCl/$NaCO_3$), and theoretical calculation of pH value and competitive anions on the desorption of $Bi_4I_2O_5$. This material is available free of charge via the Internet at http://pubs.acs.org/.

■ AUTHOR INFORMATION

Corresponding Authors

*E-mail: weiyouyang@tsinghua.org.cn.
*E-mail: d.yang@qdu.edu.cn.

Notes

The authors declare no competing financial interest.

■ ACKNOWLEDGMENTS

This work is financially supported by the National Natural Science Foundation of China (21207073) and ARC Discovery Project (130104759).

■ REFERENCES

(1) Robertson, H. A.; Falconer, I. R. Accumulation of Radioactive Iodine in Thyroid Glands Subsequent to Nuclear Weapon Tests and the Accident at Windscale. *Nature* **1959**, *184*, 1699−1702.

(2) De Vathaire, F.; Drozdovitch, V.; Brindel, P.; Rachedi, F.; Boissin, J.; Sebbag, J.; Shan, L.; Bost-Bezeaud, F.; Petitdidier, P.; Paoaafaite, J. Thyroid Cancer following Nuclear Tests in French Polynesia. *Br. J. Cancer* **2010**, *103*, 1115−1121.

(3) Jaworowski, Z. UNSCEAR on the Health Effects from Chornobyl. *Science* **2001**, *293*, 605−606.

(4) Zonenberg, A.; Leoniak, M.; Zarzycki, W. The Effect of Chernobyl Accident on the Development of Non Malignant Diseases. *Endokrynol. Polym.* **2006**, *57*, 38−44.

(5) Hosoda, M.; Tokonami, S.; Tazoe, H.; Sorimachi, A.; Monzen, S.; Osanai, M.; Akata, N.; Kakiuchi, H.; Omori, Y.; Ishikawa, T.; Sahoo, S. T.; Kovács, T.; Yamada, M.; Nakata, A.; Yoshida, M.; Yoshino, H.; Mariya, Y.; Kashiwakura, I. Activity Concentrations of Environmental Samples Collected in Fukushima Prefecture Immediately after the Fukushima Nuclear Accident. *Sci. Rep.* **2013**, *3*, 2283−2288.

(6) Xu, S.; Freeman, S. P.; Hou, X.; Watanabe, A.; Yamaguchi, K.; Zhang, L. Iodine Isotopes in Precipitation: Temporal Responses to ^{129}I Emissions from the Fukushima Nuclear Accident. *Environ. Sci. Technol.* **2013**, *47*, 10851−10859.
(7) Rose, P. S.; Swanson, R. L.; Cochran, J. K. Medically-Derived ^{131}I in Municipal Sewage Effluent. *Water Res.* **2012**, *46*, 5663−5671.
(8) Pacini, F.; Schlumberger, M.; Harmer, C.; Berg, G. G.; Cohen, O.; Duntas, L.; Jamar, F.; Jarzab, B.; Limbert, E.; Lind, P.; Reiners, C.; Sanchez Franco, F.; Smit, J.; Wiersinga, W. Post-Surgical Use of Radioiodine (^{131}I) in Patients with Papillary and Follicular Thyroid Cancer and the Issue of Remnant Ablation: a Consensus Report. *Eur. J. Endocrinol.* **2005**, *153*, 651−659.
(9) Hackshaw, A.; Harmer, C.; Mallick, U.; Haq, M.; Franklyn, J. A. ^{131}I Activity for Remnant Ablation in Patients with Differentiated Thyroid Cancer: a Systematic Review. *J. Clin. Endocrinol. Metab.* **2007**, *92*, 28−38.
(10) Huang, R.; Zhao, Z.; Ma, X.; Li, S.; Gong, R.; Kuang, A. Targeting of Tumor Radioiodine Therapy by Expression of the Sodium Iodide Symporter under Control of the Survivin Promoter. *Cancer Gene Ther.* **2011**, *18*, 144−152.
(11) Rose, P. S.; Smith, J. P.; Cochran, J. K.; Aller, R. C.; Swanson, R. L. Behavior of Medically-Derived ^{131}I in the Tidal Potomac River. *Sci. Total Environ.* **2013**, *452*, 87−97.
(12) Jiménez, F.; López, R.; Pardo, R.; Debán, L.; García-Talavera, M. The Determination and Monitoring of ^{131}I Activity in Sewage Treatment Plants based on A2/O Processes. *Radiat. Meas.* **2011**, *46*, 104−108.
(13) Barquero, R.; Agulla, M.; Ruiz, A. Liquid Discharges from the Use of Radionuclides in Medicine (Diagnosis). *J. Environ. Radioact.* **2008**, *99*, 1535−1538.
(14) Fischer, H. W.; Ulbrich, S.; Pittauerová, D.; Hettwig, B. Medical Radioisotopes in the Environment-Following the Pathway from Patient to River Sediment. *J. Environ. Radioact.* **2009**, *100*, 1079−1085.
(15) Kleinschmidt, R. Uptake and Depuration of of ^{131}I by the Macroalgae Catenella Nipae-Potential use as an Environmental Monitor for Radiopharmaceutical Waste. *Mar. Pollut. Bull.* **2009**, *58*, 1539−1543.
(16) Xu, C.; Miller, E. J.; Zhang, S.; Li, H.-P.; Ho, Y.-F.; Schwehr, K. A.; Kaplan, D. I.; Otosaka, S.; Roberts, K. A.; Brinkmeyer, R.; Yeager, C. M.; Santschi, P. H. Sequestration and Remobilization of Radioiodine (^{129}I) by Soil Organic Matter and Possible Consequences of the Remedial Action at Savannah River Site. *Environ. Sci. Technol.* **2011**, *45*, 9975−9983.
(17) Atkins, M.; Glasser, F. Application of Portland Cement-Based Materials to Radioactive Waste Immobilization. *Waste Manage.* **1992**, *12*, 105−131.
(18) Aimoz, L.; Wieland, E.; Taviot-Guého, C.; Dähn, R.; Vespa, M.; Churakov, S. V. Structural Insight into Iodide Uptake by AFm Phases. *Environ. Sci. Technol.* **2012**, *46*, 3874−3881.
(19) Bo, A. Development of Modified Inorganic Adsorbents for Radioactive Iodine Removal and Biomolecule Adsorption. *MS Thesis*, Queensland University of Technology, Brisbane, Australia, 2012.
(20) Lokhande, R. S.; Singare, P. U.; Dole, M. H. Comparative Study on Bromide and Iodide Ion-Isotopic Exchange Reactions using Strongly Basic Anion Exchange Resin Duolite A-113. *J. Nucl. Radiochem. Sci.* **2006**, *7*, 29−32.
(21) Taylor, P.; Lopata, V. J. Equilibria between Bi_2O_3 and Bi_5O_7I in Aqueous Solutions at 10−60 °C, and in Oxygen Atmospheres at 550−800 °C. *Can. J. Chem.* **1988**, *66*, 2664−2670.
(22) Kodama, H. Removal of Iodide Ion from Simulated Radioactive Liquid Waste. *Czech. J. Phys.* **1999**, *49*, 971−977.
(23) Balsley, S. D.; Brady, P. V.; Krumhansl, J. L.; Anderson, H. L. Iodide Retention by Metal Sulfide Surfaces: Cinnabar and Chalcocite. *Environ. Sci. Technol.* **1996**, *30*, 3025−3027.
(24) Grambow, B. Mobile Fission and Activation Products in Nuclear Waste Disposal. *J. Contam. Hydrol.* **2008**, *102*, 180−186.
(25) Lefevre, G.; Walcarius, A.; Ehrhardt, J.-J.; Bessiere, J. Sorption of Iodide on Cuprite (Cu_2O). *Langmuir* **2000**, *16*, 4519−4527.
(26) Lefèvre, G.; Bessière, J.; Ehrhardt, J.-J.; Walcarius, A. Immobilization of Iodide on Copper (I) Sulfide Minerals. *J. Environ. Radioact.* **2003**, *70*, 73−83.
(27) Yang, D.; Liu, H.; Zheng, Z.; Sarina, S.; Zhu, H. Titanate-Based Adsorbents for Radioactive Ions Entrapment from Water. *Nanoscale* **2013**, *5*, 2232−2242.
(28) Yang, D.; Liu, H.; Liu, L.; Sarina, S.; Zheng, Z.; Zhu, H. Silver Oxide Nanocrystals Anchored on Titanate Nanotubes and Nanofibers: Promising Candidates for Entrapment of Radioactive Iodine Anions. *Nanoscale* **2013**, *5*, 11011−11018.
(29) Yang, D.; Sarina, S.; Zhu, H.; Liu, H.; Zheng, Z.; Xie, M.; Smith, S. V.; Komarneni, S. Capture of Radioactive Cesium and Iodide Ions from Water by Using Titanate Nanofibers and Nanotubes. *Angew. Chem., Int. Ed.* **2011**, *50*, 10594−10598.
(30) Bo, A.; Sarina, S.; Zheng, Z.; Yang, D.; Liu, H.; Zhu, H. Removal of Radioactive Iodine from Water Using Ag_2O Grafted Titanate Nanolamina as Efficient Adsorbent. *J. Hazard. Mater.* **2013**, *246*, 199−205.
(31) Krumhansl, J. L.; Nenoff, T. M. Hydrotalcite-like Layered Bismuth-Iodine-Oxides as Waste Forms. *Appl. Geochem.* **2011**, *26*, 57−64.
(32) Nenoff, T.; Krumhansl, J. L.; Rajan, A. In-Situ Formation of Bismuth-Based Iodine Waste Forms. *Mater. Res. Soc. Symp. Proc.* **2008**, *1043*, 12−05.
(33) Mascarelli, A. L. Funding Cut for US Nuclear Waste Dump. *Nature* **2009**, *458*, 1086−1087.
(34) Xie, J. S.; Li, L. S.; Tian, C.; Han, C. L.; Zhao, D. F. Template-Free Synthesis of Hierarchical Constructed Flower-like δ-Bi_2O_3 Microspheres with Photocatalytic Performance. *Micro Nano Lett.* **2012**, *7*, 651−653.
(35) Yu, Z.; Zhang, J.; Zhang, H.; Shen, Y.; Xie, A.; Huang, F.; Li, S. Facile Solvothermal Synthesis of Porous Bi_2O_3 Microsphere and their Photocatalytic Performance under Visible Light. *Micro Nano Lett.* **2012**, *7*, 814−817.
(36) Liu, Q.-C.; Ma, D.-K.; Hu, Y.-Y.; Zeng, Y.-W.; Huang, S.-M. Various Bismuth Oxyiodide Hierarchical Architectures: Alcohothermal-Controlled Synthesis, Photocatalytic Activities, and Adsorption Capabilities for Phosphate in Water. *ACS Appl. Mater. Interfaces* **2013**, *5*, 11927−11934.
(37) Kodama, H. Solidification of Iodide Ion by Reaction with Bi_2O_3. *Bull. Chem. Soc. Jpn.* **1992**, *65*, 3011−3014.
(38) Fan, H. T.; Pan, S. S.; Teng, X. M.; Ye, C.; Li, G. H.; Zhang, L. D. δ-Bi_2O_3 Thin Films Prepared by Reactive Sputtering: Fabrication and Characterization. *Thin Solid Films* **2006**, *513*, 142−147.
(39) Teterin, Y. A.; Ivanov, K.; Teterin, A. Y.; Lebedev, A.; Utkin, I.; Vukchevich, L. Auger and X-ray Photoelectron Spectroscopy Study of the Density of Oxygen States in Bismuth, Aluminium, Silicon and Uranium Oxides. *J. Electron Spectrosc. Relat. Phenom.* **1999**, *101*, 401−405.
(40) Xiao, X.; Zhang, W.-D. Hierarchical $Bi_7O_9I_3$ Micro/Nano-Architecture: Facile Synthesis, Growth Mechanism, and High Visible Light Photocatalytic Performance. *RSC Adv.* **2011**, *1*, 1099−1105.
(41) Yu, C.; Yu, J. C.; Fan, C.; Wen, H.; Hu, S. Synthesis and Characterization of Pt/BiOI Nanoplate Catalyst with Enhanced Activity under Visible Light Irradiation. *Mater. Sci. Eng., B* **2010**, *166*, 213−219.
(42) Au, C.; Hirsch, W.; Hirschwald, W. Adsorption and Interaction of Carbon Dioxide, Formic Acid and Hydrogen/Carbon Dioxide Mixtures on (1010) Zinc Oxide Surfaces Studied by Photoelectron Spectroscopy (XPS and UPS). *Surf. Sci.* **1988**, *199*, 507−517.
(43) Wang, Y.; Wen, Y.; Ding, H.; Shan, Y. Improved Structural Stability of Titanium-Doped β-Bi_2O_3 during Visible-Light-Activated Photocatalytic Processes. *J. Mater. Sci.* **2010**, *45*, 1385−1392.
(44) Hardcastle, F. D.; Wachs, I. E. The Molecular Structure of Bismuth Oxide by Raman Spectroscopy. *J. Solid State Chem.* **1992**, *97*, 319−331.
(45) Fan, H.; Teng, X.; Pan, S.; Ye, C.; Li, G.; Zhang, L. Optical Properties of δ-Bi_2O_3 Thin Films Grown by Reactive Sputtering. *Appl. Phys. Lett.* **2005**, *87*, 231916.

(46) Punia, R.; Kundu, R.; Hooda, J.; Dhankhar, S.; Dahiya, S.; Kishore, N. Effect of Bi_2O_3 on Structural, Optical, and Other Physical Properties of Semiconducting Zinc Vanadate Glasses. *J. Appl. Phys.* **2011**, *110*, 033527.
(47) Hrizi, C.; Samet, A.; Abid, Y.; Chaabouni, S.; Fliyou, M.; Koumina, A. Crystal Structure, Vibrational and Optical Properties of A New Self-Organized Material Containing Iodide Anions of Bismuth (III),$[C_6H_4(NH_3)_2]_2Bi_2I_{10}\cdot 4H_2O$. *J. Mol. Struct.* **2011**, *992*, 96−101.
(48) Kanchana, G.; Arivuoli, D. Spectroscopic Investigation of BiSeI, SbSeI Compounds and $BiSbS_xSe_{1-x}I$ Solid Solutions. *Indian J. Eng. Mater. S.* **2001**, *8*, 373−376.
(49) Ho, Y.-S.; McKay, G. Sorption of Dye from Aqueous Solution by Peat. *Chem. Eng. J.* **1998**, *70*, 115−124.
(50) Ho, Y.-S.; McKay, G. Pseudo-Second Order Model for Sorption Processes. *Process Biochem.* **1999**, *34*, 451−465.
(51) Taylor, P.; Lopata, V. J.; Wood, D. D.; Yacyshyn, H. Solubility and Stability of Inorganic Iodides: Candidate Waste Forms for Iodine-129. *Spec. Technol. Publ.* **1989**, *1033*, 287−301.